



## Eruption conditions of spatter deposits

Erika Rader<sup>a,\*</sup>, Dennis Geist<sup>b</sup>

<sup>a</sup> School of the Environment, Washington State University, PO Box 642812, Pullman WA 99164-2812, USA

<sup>b</sup> Geological Sciences, University of Idaho, 875 Perimeter Drive, Moscow, ID 83844, USA



### ARTICLE INFO

#### Article history:

Received 20 April 2015

Accepted 2 September 2015

Available online 12 September 2015

Editor: G. Chiodini

#### Keywords:

Spatter

Clastogenic

Accumulation rate

Cooling rate

Basalt

### ABSTRACT

Spatter is an eruptive product that forms within a narrow range of thermal conditions: it must be hot enough to deform and agglutinate, but not so hot that clasts completely re-fuse and remobilize as clastogenic lava. This narrow thermal window of spatter-forming conditions allows for quantitative prediction of cooling rates and accumulation rates. Cooling and accumulation rates then provide information that enables estimates of eruption parameters for inaccessible and prehistoric deposits. High-temperature experiments conducted on basaltic scoria from Devil's Garden, Oregon have revealed the eruption temperature was ~1130 °C. The strength welds formed between experimental clasts is shown to depend on cooling rate. Natural samples are compared to the experimental samples by measuring tensile strength and welded area between clasts. The weld strength in natural deposits yields estimates of cooling rates that range between 2.5 °C and 48 °C/min, with the majority of the samples grouping between 7 °C and 14 °C/min. Thermal models based on these cooling rates yield spatter accumulation rates of 0.5–1.8 m/h in the Devil's Garden spatter deposits. We provide a general model for cooling and accumulation rates for spatter cones, ramparts, and hornitos, which allow estimation of the factors that control basaltic eruptive products.

© 2015 Elsevier B.V. All rights reserved.

### 1. Introduction

The emplacement of spatter is characteristic of almost all Hawaiian and Strombolian-style explosive eruptions, and airborne transport of molten material is a significant hazard in the near-vent environment. Moreover, if spatter accumulates quickly enough, the pile can fail structurally, as occurred at the Izu-Oshima volcano in Japan in 1986 or at Pu'u'Ō'ō, in Hawaii, during 1983–1986 (Wolfe, 1988; Sumner, 1998).

Determining the accumulation rates of spatter can provide information about the eruptive flux (Sumner et al., 2005), which is one of the most important parameters for gauging eruptive behavior. Currently, accumulation rates and eruptive fluxes for unwitnessed eruptions are virtually impossible to quantify. The presence of spatter may allow for the calculation of an accumulation rate that can be related to flux and characterize prehistoric eruptions.

Spatter is defined as an accumulation of fluid pyroclasts that agglutinate on landing (Sumner et al., 2005). Agglutination occurs when the temperatures of the clasts' exteriors are higher than the glass transition, which ranges between 500 °C and 739 °C for basalt, depending on the cooling rate (Giordano et al., 2005). Above the glass transition temperature, glass deforms and anneals, which can result in clasts interfusing. Owing to this constraint, the extent of fusing of spatter provides the opportunity to quantify the conditions that are characteristic of basaltic eruptions, specifically accumulation and cooling rates (Sumner et al.,

2005). Currently, only a qualitative relationship between spatter production, cooling rate, and accumulation rate is understood (e.g. the regime diagram of Sumner et al., 2005).

In the continuum between fluid lava and fully solidified pyroclasts, spatter may be categorized in a 1–5 scale (Sumner et al., 2005). Type 1 clasts are undeformed and unfused, thus are solid and brittle by the time they land (normal scoria). Type 2 clasts have brittle rims, but are still molten on the inside when they land. Type 3 clasts agglutinate upon landing and have molten interiors. Type 4 clasts are so fluid that they splash upon impact and coalesce to form a clastogenic lava. Type 5 clasts have a brittle core, yet a fluid rim, and are produced by the recycling of scoria in a fountain. We focus on accumulation and cooling rates that will produce type 3 clasts by combining field studies, experiments, and thermal models of spatter features at the vent complex of Devil's Garden, Oregon, USA, a Holocene lava field. Because agglutinated spatter deposits form in a narrow range of accumulation and cooling rates, these methods are potentially applicable to eruption rates of unobserved basaltic eruptions (Fagents and Wilson, 1994; Fagents, 1996; Hauber et al., 2009).

### 2. Background

#### 2.1. Field site

Devil's Garden is a basaltic lava flow field located ~40 km southeast of Bend, Oregon (Fig. 1; Keith et al., 1988; Chitwood, 1994). The lava field of Devil's Garden is part of the High Lava Plains province, which

\* Corresponding author.

E-mail address: [Erika.rader@wsu.edu](mailto:Erika.rader@wsu.edu) (E. Rader).

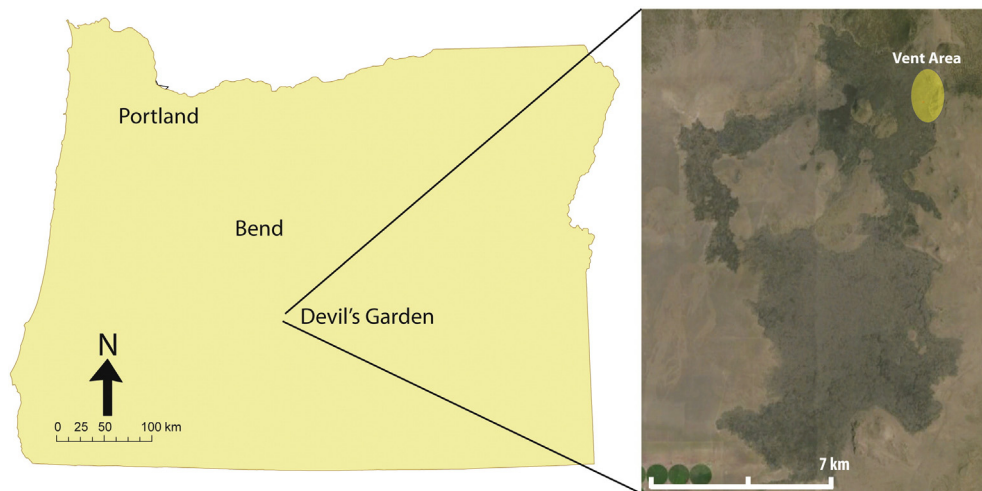


**Fig. 1.** Location map of Devil's Garden Volcanic Field. The lava field is located about 80 km SE of Bend, OR. In the blow-up, the region shaded yellow is where the three spatter localities are found.

is thought by some to be linked to the Yellowstone hotspot (Jordan et al., 2004). The basaltic fissures are oriented N–S, however, suggesting basin and range control (Christiansen et al., 2002). Devil's Garden is younger than the Holocene volcanic rocks on which it sits (<15,000 years) but older than the eruption of Mt. Mazama at  $7527 \pm 150$  yBP (Zdanowicz et al., 1999). Chemical analyses of two samples, USGS sample name C159387 and C159389, are in Table 1.

Three vents erupted spatter deposits within the Devil's Garden volcanic field. The main vent is located at the farthest northeastern corner of the lava field, which totals  $\sim 1.2 \text{ km}^3$  of basalt. The main vent complex is a  $\sim 10$ -m-high elongated scoria cone oriented north–south. The outer flanks of the cone are made up of scoriaceous lapilli and the inner walls of the summit crater expose dozens of layers of 5- to 10-cm-thick lavas. The lavas are thin and laterally continuous over a few meters, with spongy interiors and glassy rims. Most of the spatter at the main vent is located at the northwest corner of the cone. At this location, isolated clasts predominantly between 5 and 15 cm in diameter have porous cores and quenched rims. Twisted lobes, impressions of other clasts on the underside of blobs, fusiform shapes, and droopy forms indicate both pre- and post-depositional plastic deformation. This spatter pile is <2 m thick and extends for about 3 m horizontally along the top of the scoria cone. Most of these clasts preserve evidence of having been fluid when deposited, but they are not strongly agglutinated. According to the scheme of Sumner et al. (2005), most clasts are Type 2.

Another spatter deposit at Devil's Garden is a vent complex 1.7 km south of the main vent called "the Blowouts" (Erickson et al., 1989).

**Table 1**  
Chemical analyses of Devil's Garden lava.

| wt. %                          | Sample  |         |
|--------------------------------|---------|---------|
|                                | C159387 | C159389 |
| SiO <sub>2</sub>               | 47.7    | 49.3    |
| TiO <sub>2</sub>               | 1.61    | 1.48    |
| Al <sub>2</sub> O <sub>3</sub> | 16.6    | 16.7    |
| Fe <sub>2</sub> O <sub>3</sub> | 10.7    | 10.5    |
| MgO                            | 9.19    | 8.83    |
| CaO                            | 9.78    | 9.43    |
| Na <sub>2</sub> O              | 2.97    | 2.95    |
| K <sub>2</sub> O               | 0.58    | 0.6     |
| P <sub>2</sub> O <sub>5</sub>  | 0.41    | 0.42    |

From USGS database ([http://mrddata.usgs.gov/ngdb/rock/show-ngdbrock.php?lab\\_id=C159387](http://mrddata.usgs.gov/ngdb/rock/show-ngdbrock.php?lab_id=C159387)).

Two steep-sided spatter cones rise  $\sim 20$  m and share a border (Fig. 2). The southern structure is smaller and has a narrow breach  $\sim 10$  m wide that allowed ponded lava to flow into the larger northern cone and escape through a breached western rim. The interior walls of the Blowouts are almost entirely constituted of spatter. A thin layer of scoria coats the outer flanks, but scoria is very sparse in the stratigraphy exposed by the crater walls.

Spatter bombs are elongate with the long axis ranging from 5 to 50 cm, and are between 3 and 10 cm thick, and are dominantly Type 2 and 3 clasts (Fig. 3). The clasts have glassy rinds containing <0.1 mm undeformed vesicles, while their cores are highly vesicular and have an abundance of irregular, coalesced vesicles. The bulk of the volume of these deposits consists of contorted and spinose bombs, some of which are so strongly fused that it is difficult to distinguish individual bombs without exposing their vesiculated interiors and barely perceptible rinds. The voids between bombs are irregular and aligned randomly, indicating no strong horizontal simple shear (such as down-slope creep).

The third location of spatter that we studied is a 150-m-long zone of fissures that built up small spatter ramparts and hornitos between the main vent and the Blowouts. A very well-formed hornito on the west side of the road is  $\sim 3$  m across and 1.5 m tall, with nearly vertical walls. Spatter clasts are less contorted than those at the Blowouts or the main vent, likely due to the shorter flight path (about 1 m), but they are Type 3 clasts.



**Fig. 2.** Aerial image of the Blowouts, Devil's Garden. This Google Earth image shows the orientation of these secondary vents, which produced small lava flows out to the west, as indicated by the white arrow.

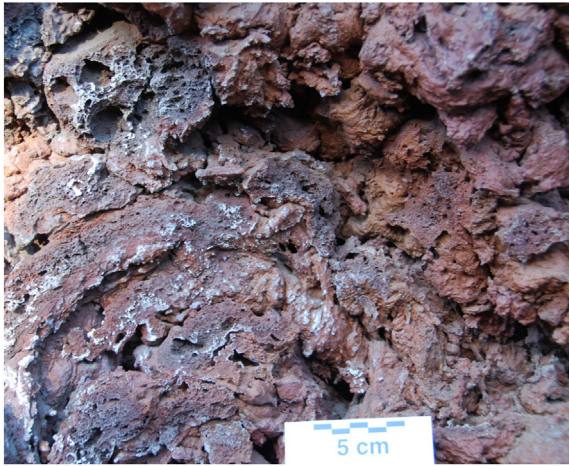


**Fig. 3.** Photo of cross-section of spatter pile at the Blowouts. Clasts can be hard to distinguish from one another without a view of the vesiculated core because they are so contorted and fused together.

## 2.2. Cooling rates of spatter

Slower cooling rates result in a lower glass transition temperature with cooling rates of 1 °C–10 °C/min producing glass transition temperatures of 500 °C–739 °C (Giordano et al., 2005). One method to estimate cooling rates in volcanic glasses is relaxational geospeedometry (Wilding et al., 1996), which identifies the glass transition temperature by a sharp increase in heat capacity. Cooling rate can then be calculated, as the transition temperature is defined as the point when the cooling rate exceeds the rate at which the glass can deform. One study using this method found phonolite bombs from Tenerife with cooling rates as high as 600 °C/min on the rim of bombs and as low as 0.002 °C/min at their core (Wilding et al., 1996). Glassy rims on pillow basalts also cool very quickly having rates that range from 6 °C to 4,332 °C/min (72.2 °C/s) (e.g. Bowles et al., 2005; Nichols et al., 2009). Subaerial basaltic lavas, analyzed by the same technique as well as measured directly by thermal infrared spectroscopy, exhibit cooling rates from 8 °C/min to 140 °C/min for lava exposed to the atmosphere to as low as 0.2 °C–0.8 °C/min for lava transported in insulated channels (Cashman et al., 1999; Gottsmann et al., 2004). Spatter-fed phonolitic obsidian clastogenic flows exhibit slower cooling rates between 0.039 and 0.0028 °C/min (Gottsmann and Dingwell, 2001). Despite having a pyroclastic origin, these measurements from obsidian provide a lower limit to possible cooling rates, because the glass is completely annealed, possibly due to greater reservoir of heat in the thick dense flows. Surficial heat loss of a stable surface crust of lava, on the other hand, represents the fastest cooling rate possible for air-cooled deposits. In sum, on the basis of measurements of other types of material, we conclude that cooling rates for basaltic spatter are expected to fall between 0.039 °C/min and 140 °C/min.

## 3. Methods

Spatter scoria bombs ~25 cm in diameter were collected and cut into ~2.5 cm<sup>3</sup> cubes. The starting material had a vesicularity that ranged between 7% and 45%, and the vesicles were typically 1–5 mm in diameter. Thirty-seven heating experiments were first performed on single lava cubes to assess their deformation under their own weight as a function of temperature. No deformation was observed below 1120 °C. The lava deforms ductilely at 1125 °C and is highly fluid at 1140 °C. Therefore, the controlled cooling experiments were all initiated at 1130 °C, which provides the ideal experimental condition to induce welding on a small scale over a short period of time.

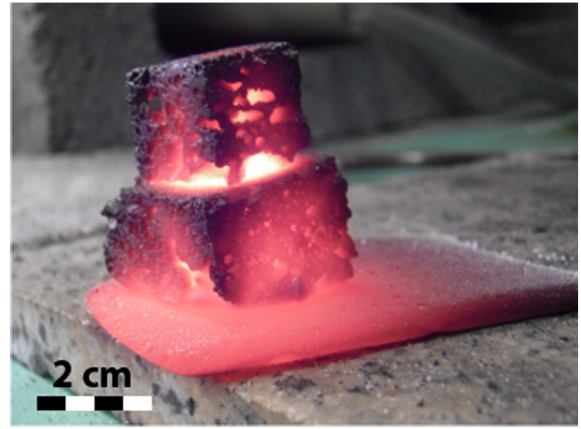


**Fig. 4.** Cubes of samples stacked on a graphite plate. These had been heated in a tube furnace at 1130 °C for 30 min, then were cooled below 300 °C at cooling rates between 1 °C/min and 10 °C/min.

To simulate cooling and annealing of spatter under controlled conditions, we ran experiments on natural basalt clasts collected from Devil's Garden. Two cut cubes were stacked on a graphite plate and inserted into a preheated tube furnace (Fig. 4). Samples were maintained at temperatures ranging from 1000 °C to 1140 °C for 20 to 120 min. After extraction from the tube furnace and a short (10 to 20 s) exposure to room temperatures during transfer, the scoria cubes were cooled in a muffle furnace programmed with specific cooling rates ranging from 1 °C/min to 10 °C/min between the temperatures of 1100 °C and 300 °C. After the sample was cooled to 300 °C, the experiments were quenched by shutting off power to the muffle furnace.

Experiments which exhibited a welded surface between the two cubes were subjected to tension tests once cooled to determine the strength of the weld. Hooks were bonded onto the ends of the cubes with Devcon 3500 psi epoxy and allowed to cure overnight. A spring scale with a 22.7 kg capacity and a 0.2 kg sensitivity measured the force required to reach the failure point. The sample apparatus was placed under increasing tension until failure of the weld occurred. If failure occurred along a microfracture inside one of the two cubes instead of along the weld, the experiment was disregarded. Each trial was filmed to capture the force exerted on each sample accurately. The freshly broken weld where the cubes had been connected was photographed and the surface area that had been in contact between the two cubes was measured. Several experiments were excluded from the analysis because they were dropped, melted completely, or there were difficulties maintaining the temperature for the entire duration of the fusing phase of the experiment. In several excluded samples, epoxy dripped between the two cubes.

## 4. Results

Groundmass collected 5 mm inside the glazed rim of eleven spatter clasts from all three vent localities at Devil's Garden have crystallinities estimated between 20% and 40% (Table 2). The crystals are plagioclase (10%–20%), pyroxene (2%–10%), and olivine (0%–7%). There is a widely variable amount of Fe-oxide microlites in the different samples (1%–13%). Olivine and pyroxene are strongly oxidized (black opaque oxide replacement) in spatter samples H-12-02A, BO-12-01, and BO-12-02. Plagioclase crystals are subhedral and 0.4–0.9 mm long. The groundmass of the cores (within a few mm of the rim) of these spatter clasts contains little glass and numerous microlites of Fe-oxide and plagioclase.

### 4.1. Annealing experiments

Maximum eruption temperature of spatter deposits was constrained by melting experiments, which illustrated that total structural integrity

**Table 2**  
Modal mineralogy of spatter clasts from Devil's Garden.

| Sample    | Groundmass | Feldspar |           | Pyroxene |           | Olivine |           | Oxide |
|-----------|------------|----------|-----------|----------|-----------|---------|-----------|-------|
|           |            | Mode     | Size (mm) | Mode     | Size (mm) | Mode    | Size (mm) |       |
| H-12-01A  | 65         | 10       | 0.6       | 10       | 0.4       | 7       | 0.4       | 8     |
| H-12-01B  | 65         | 15       | 0.9       | 10       | 0.3       | 5       | 0.7       | 5     |
| H-12-01C  | 65         | 10       | 0.4       | 10       | 0.3       | 5       | 0.4       | 10    |
| H-12-02A  | 70         | 15       | 0.5       | 4        | 0.4       | 1       | 0.7       | 10    |
| H-12-02B  | 70         | 15       | 0.5       | 4        | 0.5       | 1       | 0.3       | 10    |
| H-12-02C  | 70         | 15       | 0.5       | 4        | 0.3       | 1       | 0.3       | 10    |
| BO-12-01  | 60         | 20       | 0.5       | 10       | 0.4       | 4       | 0.4       | 6     |
| BO-12-02  | 80         | 10       | 0.5       | 5        | 0.3       | 4       | 0.4       | 1     |
| BO-12-03A | 69         | 16       | 0.7       | 8        | 0.4       | 2       | 0.4       | 5     |
| BO-12-03B | 80         | 10       | 0.7       | 5        | 0.5       | 4       | 0.6       | 1     |
| BO-12-03C | 80         | 10       | 0.6       | 5        | 0.4       | 4       | 1         | 1     |

of the cube was lost at 1140 °C. Similarly, the glass transition temperature signals the minimum temperature of agglutination. The glass transition temperature of basalt of this composition is between 500 °C and 739 °C, depending on the cooling rate and water content (Giordano et al., 2005). Spatter deposits, therefore, must be deposited above the glass transition temperature. Several studies have documented the temperature of active basaltic spatter eruptions. At Erta'Ale volcano, humidity-corrected thermal imaging measured temperatures of fountaining spatter between 1140 °C and 1012 °C with an average of 1084 °C (Davies et al., 2011). Thermocouple measurements of fountaining lava at Surtsey yielded temperatures of 1100 °C to 1140 °C (Einarsson, 1966; Sigurgeirsson, 1966). Single-cube experiments from this study provide a structural melting point that preserves the natural phenocryst population, hence maximum, eruption temperature of 1135 °C.

Welding experiments included 12 pairs of cubes held at a fixed cooling rate (1, 2, 3, 5, or 10°/min (Table 3). We found the tensile strength of the experimental welds to range from 1.5 to 15.3 N/mm<sup>2</sup>. Weld strength increased with decreasing cooling rate (Fig. 5). We estimate the uncertainty for the strength of the weld based on  $n = 5$  runs at a single cooling rate to be 3.3 N/mm<sup>2</sup> (1 $\sigma$ ). Three other sets of replicates were well within this range.

Weld strength can then be measured on natural spatter, to deduce the post-deposition cooling rate. Naturally welded spatter clasts collected from Devil's Garden were measured to be between 0.6 and 6.9 N/mm<sup>2</sup> (Table 3). Four of the six naturally welded samples have estimated cooling rates ranging from 6.8 °C/min to 14 °C/min (Fig. 6). The only other estimate of cooling rates of spatter deposits that we are aware

of comes from phonolitic obsidian spatter, which is chemically and physically very different from the basalt studied here. Gottsmann and Dingwell (2001) used glass transition to estimate cooling rates of 0.039 °C/min and 0.0028 °C/min, which are much lower than Devil's Garden basaltic spatter. We note that Gottsmann and Dingwell's cooling rates are low, and may be due to the physical setting of the flows and the compositions of those magmas. Devil's Garden spatter cooling rates are also much faster than those measured from the interior of lavas (Gottsmann et al., 2004).

#### 4.2. Accumulation rates of spatter

Accumulation rate is known to be one of the most important factors that governs the construction and thermal evolution of spatter deposits (Thomas and Sparks, 1992; Sumner et al., 2005), because the stacking of hot clasts slows cooling of the deposit. Accumulation rates have been measured at a few spatter-producing eruptions. At Izu-Oshima volcano, a spatter pile accumulated so quickly that it became clastogenic after having accumulated at 10.2 m/h, indicating that this might be near the transition between the clastogenic and spatter regimes (type 2–5 clasts that fail under their own weight; Sumner, 1998). Experiments on actively forming scoria cones yield accumulation rates that range from ~1 to 5 m/h (Riedel et al., 2003).

To calculate accumulation rate of spatter from estimated cooling rates, the implicit, finite-difference cooling model of Gerya (2010) was modified to simulate a vesiculated basaltic spatter clast deposited on cool ground. Cooling occurs from the top by natural convection with air and through the bottom by conduction into the ground. The model is one-dimensional, so heat transfer through the sides of the clast is

**Table 3**  
Experimental and natural cooling rates of spatter.

| Sample name | Sample type | Failure point (N) | Contact surface area (mm <sup>2</sup> ) | N/mm <sup>2</sup> | Cooling rate (°C/min) |
|-------------|-------------|-------------------|---|-------------------|-----------------------|
| H2F-10B     | Experiment  | 31.1              | 2                                       | 15.5              | <sup>a</sup> 1        |
| H5A-1A      | Experiment  | 22.2              | 1.5                                     | 14.9              | <sup>a</sup> 1        |
| H2F-8       | Experiment  | 66.7              | 15.1                                    | 4.4               | <sup>a</sup> 2        |
| H2F-9       | Experiment  | 40                | 9.9                                     | 4                 | <sup>a</sup> 2        |
| H5A-3A      | Experiment  | 31.1              | 2.8                                     | 11.3              | <sup>a</sup> 2        |
| H1A4        | Experiment  | 4.4               | 0.4                                     | 10.3              | <sup>a</sup> 2        |
| H1A3        | Experiment  | 6.7               | 0.7                                     | 9                 | <sup>a</sup> 2        |
| H5A-4A      | Experiment  | 40                | 3.8                                     | 10.6              | <sup>a</sup> 3        |
| H1A2        | Experiment  | 20                | 1.8                                     | 11.3              | <sup>a</sup> 3        |
| H2D-25      | Experiment  | 8.9               | 2.9                                     | 3.1               | <sup>a</sup> 5        |
| H2E-1       | Experiment  | 149               | 55                                      | 2.7               | <sup>a</sup> 10       |
| H2E-3       | Experiment  | 16                | 11                                      | 1.5               | <sup>a</sup> 10       |
| H2-N2       | Natural     | 40                | 5.8                                     | 6.9               | <sup>b</sup> 2.5      |
| H1-N4       | Natural     | 62.3              | 20.8                                    | 3                 | <sup>b</sup> 6.8      |
| H1-N5       | Natural     | 26.7              | 9.3                                     | 2.9               | <sup>b</sup> 7.2      |
| H5-N6       | Natural     | 57.8              | 25                                      | 2.3               | <sup>b</sup> 9.2      |
| H2-N1       | Natural     | 37.8              | 23.7                                    | 1.6               | <sup>b</sup> 14.3     |
| H1-N1       | Natural     | 24.5              | 43                                      | 0.6               | <sup>b</sup> 48.4     |

<sup>a</sup> Monitored by thermocouple.

<sup>b</sup> Calculated from experiments.

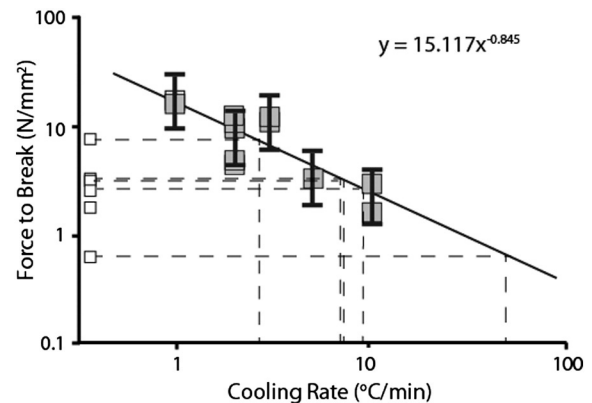


**Fig. 5.** The tensile strength of artificial welds shows a strong anticorrelation to the cooling rate of spatter. Experiments are in grey squares and natural samples in white squares connected by dashed lines to the line fitted to the experimental data. Error bars are equal to 1 standard deviation of the 5 experiments repeated at a cooling rate of 2 °C/min. All other repeats were below this standard deviation.

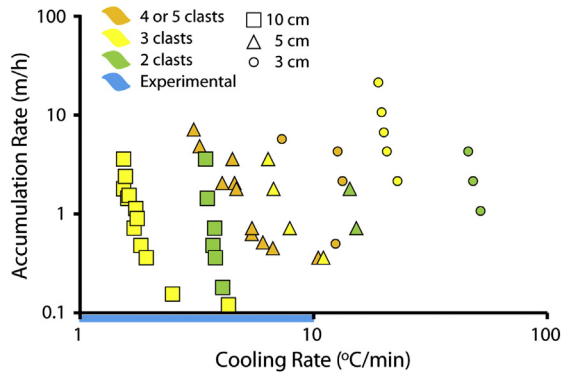


**Fig. 6.** Model of the interrelationship of accumulation rate, deposit thickness, and clast size. Cooling rate anticorrelates to accumulation rate, but clast diameter and total thickness are stronger controls. Colors represent the number of clasts deposited (orange, 4 or 5 in a row; yellow, 3 in a row; and green, 2 in a row). Shape represents the thickness of the clast (squares, 10 cm; triangles, 5 cm; circles, 3 cm).

neglected. The model periodically deposits a new clast on top of the growing pile. The thickness of clasts in the model varies between 3 and 10 cm, the range of thicknesses of clasts at Devil's Garden. These assumptions allow us to use the one-dimensional heat flow equation:

$$\frac{\delta^2 T}{\delta x^2} - \frac{1}{k} \frac{\delta T}{\delta t} = 0$$

where  $T$  is temperature,  $x$  is position,  $\kappa$  is thermal diffusivity, and  $t$  is time (latent heat of crystallization and exsolution are neglected). The parameters used in the model are in Table 4. The equation was solved for temperature as a function of time using a finite element method and starting with initial conditions  $T(t = 0, x) = 20\text{ °C}$  for the ground below the pile and the air above the pile the clast pile and  $T(t = 0, x) = 1130\text{ °C}$  for the clast pile. The deposition temperature is based on the hottest temperature achieved before total relaxation of the experimental cubes. Hot clasts are then added to the top of the pile after a designated time interval to study the effects of such a thermal perturbation on the deposit as a whole.

Modeled cooling rates of the bulk deposit between the temperatures of 1130 °C and 630 °C range from 1.5 °C/min for 10 cm clasts being deposited every 100 s to 52 °C/min for 3 cm clasts deposited every 100 s (Fig. 6; Table 5). As expected, cooling rates correlate with accumulation rate, but the thickness of individual clasts has a stronger control on cooling rate than accumulation rate.

This thermal model allows one to calculate the accumulation rate for the blowouts at Devil's Garden based on the experimental cooling rate simulations (Table 3), estimates of the initial temperature (1130 °C), and measurement of the size of the clasts in the field. This yields accumulation rates for spatter clasts (5 cm in thickness) of 0.5 to 1.8 m/h and cooling rates between 6.8 °C/s and 14.3 °C/s (Fig. 7). The two outliers in the natural samples, 2.5 °C/min and 48.4 °C/min, require different conditions. A cooling rate of 2.5 °C/min corresponds to 10-cm-thick clasts accumulating at a rate of 0.2 m/h, while to achieve a cooling rate of 48.4 °C/min, the model required an accumulation rate of 2.2 m/h of 3-cm-thick clasts. This suggests that the cooling rates will vary within

**Table 4**  
Thermal constants used in model.

| Symbol | Parameter                 | Value | Units                              | Source                     |
|--------|---------------------------|-------|------------------------------------|----------------------------|
| K      | Thermal conductivity      | 1     | W m <sup>-1</sup> K <sup>-1</sup>  | Robertson and Peck, (1974) |
| Cp     | Specific heat             | 1490  | J kg <sup>-1</sup> K <sup>-1</sup> | Robertson, (1988)          |
| rho    | Density                   | 1300  | kg m <sup>-3</sup>                 | This study                 |
| H      | Heat Transfer Coefficient | 8     | J m <sup>-3</sup>                  | Harris et al., (2005)      |

**Table 5**  
Cooling rates for modeled accumulation rates.

| $n_{clasts}$ | $d_{clast}$<br>(m) | $d_{deposit}$<br>(m) | $t_{clast}$<br>(s) | $t_{next}$<br>(s) | Cooling rate<br>(°C/min) | Accumulation<br>(m/h) |
|--------------|--------------------|----------------------|--------------------|-------------------|--------------------------|-----------------------|
| 1            | 0.05               | 0.05                 | –                  | –                 | 125                      | –                     |
| 1            | 0.1                | 0.1                  | –                  | –                 | 31                       | –                     |
| 2            | 0.03               | 0.06                 | 25                 | –                 | 45.9                     | 4.3                   |
| 2            | 0.03               | 0.06                 | 50                 | –                 | 48.1                     | 2.2                   |
| 2            | 0.03               | 0.06                 | 100                | –                 | 51.8                     | 1.1                   |
| 2            | 0.05               | 0.1                  | 100                | –                 | 14.3                     | 1.8                   |
| 2            | 0.05               | 0.1                  | 250                | –                 | 15.2                     | 0.7                   |
| 2            | 0.1                | 0.2                  | 100                | –                 | 3.4                      | 3.6                   |
| 2            | 0.1                | 0.2                  | 250                | –                 | 3.5                      | 1.4                   |
| 2            | 0.1                | 0.2                  | 500                | –                 | 3.8                      | 0.7                   |
| 2            | 0.1                | 0.2                  | 750                | –                 | 3.7                      | 0.5                   |
| 2            | 0.1                | 0.2                  | 1000               | –                 | 3.8                      | 0.4                   |
| 2            | 0.1                | 0.2                  | 1000               | –                 | 3.8                      | 0.4                   |
| 2            | 0.1                | 0.2                  | 2000               | –                 | 4.1                      | 0.2                   |
| 3            | 0.03               | 0.09                 | 5                  | 5                 | 18.9                     | 21.6                  |
| 3            | 0.03               | 0.09                 | 10                 | 10                | 19.5                     | 10.8                  |
| 3            | 0.03               | 0.09                 | 16                 | 16                | 19.9                     | 6.8                   |
| 3            | 0.03               | 0.09                 | 25                 | 25                | 20.6                     | 4.3                   |
| 3            | 0.03               | 0.09                 | 50                 | 50                | 22.8                     | 2.2                   |
| 3            | 0.05               | 0.15                 | 50                 | 50                | 6.4                      | 3.6                   |
| 3            | 0.05               | 0.15                 | 100                | 100               | 6.7                      | 1.8                   |
| 3            | 0.05               | 0.15                 | 250                | 250               | 7.9                      | 0.7                   |
| 3            | 0.05               | 0.15                 | 500                | 500               | 11                       | 0.4                   |
| 3            | 0.1                | 0.3                  | 100                | 250               | 1.5                      | 1.8                   |
| 3            | 0.1                | 0.3                  | 100                | 100               | 1.5                      | 3.6                   |
| 3            | 0.1                | 0.3                  | 250                | 250               | 1.6                      | 1.4                   |
| 3            | 0.1                | 0.3                  | 250                | 100               | 1.6                      | 2.4                   |
| 3            | 0.1                | 0.3                  | 500                | 500               | 1.7                      | 0.7                   |
| 3            | 0.1                | 0.3                  | 500                | 100               | 1.6                      | 1.5                   |
| 3            | 0.1                | 0.3                  | 750                | 750               | 1.8                      | 0.5                   |
| 3            | 0.1                | 0.3                  | 750                | 100               | 1.7                      | 1.1                   |
| 3            | 0.1                | 0.3                  | 1000               | 3000              | 2.5                      | 0.2                   |
| 3            | 0.1                | 0.3                  | 1000               | 1000              | 1.9                      | 0.4                   |
| 3            | 0.1                | 0.3                  | 1000               | 100               | 1.8                      | 0.9                   |
| 3            | 0.1                | 0.3                  | 3000               | 3000              | 4.3                      | 0.1                   |
| 4            | 0.03               | 0.12                 | 25                 | 25                | 12.7                     | 4.3                   |
| 4            | 0.04               | 0.16                 | 25                 | 25                | 7.3                      | 5.8                   |
| 4            | 0.04               | 0.16                 | 100                | 350               | 12.4                     | 0.5                   |
| 4            | 0.05               | 0.2                  | 25                 | 25                | 3.1                      | 7.2                   |
| 4            | 0.05               | 0.2                  | 37                 | 37                | 3.3                      | 4.9                   |
| 4            | 0.05               | 0.2                  | 50                 | 100               | 4.1                      | 2.1                   |
| 4            | 0.05               | 0.2                  | 50                 | 100               | 4.6                      | 2.1                   |
| 4            | 0.05               | 0.2                  | 50                 | 50                | 4.5                      | 3.6                   |
| 4            | 0.05               | 0.2                  | 100                | 350               | 5.4                      | 0.6                   |
| 4            | 0.05               | 0.2                  | 100                | 100               | 4.7                      | 1.8                   |
| 4            | 0.05               | 0.2                  | 250                | 250               | 5.4                      | 0.7                   |
| 4            | 0.05               | 0.2                  | 350                | 350               | 6.1                      | 0.5                   |
| 4            | 0.05               | 0.2                  | 400                | 400               | 6.7                      | 0.5                   |
| 4            | 0.05               | 0.2                  | 500                | 500               | 10.5                     | 0.4                   |
| 5            | 0.03               | 0.15                 | 50                 | 50                | 13.3                     | 2.2                   |

Headings are as follows:  $n_{clasts}$  is the number of clasts accumulated in the model run;  $d_{clast}$  is the diameter of the clasts in the run;  $d_{deposit}$  is the final depth of the spatter pile;  $t_{clast}$  is the time between the first and second clast deposition;  $t_{next}$  is the time interval between subsequent deposition of clasts; Cooling rate is calculated from the model; Accumulation rate is calculated by dividing the product of  $n_{clast}$  and  $d_{clast}$  by the total time it took to deposit all of the clasts in the run.

a deposit depending on the size of the clasts, since cooling time is a function of the ratio of surface area to volume (rims cool quickly, cores cool slowly). Given that the majority of clasts measured at Devil's Garden are 5 cm thick, eruption conditions with accumulation rates of 0.5–1.8 m/h and cooling rates of 6.8 °C/min–14.3 °C/min will produce agglutinated type 3 spatter clasts. This model shows that it is necessary to accumulate several clasts quickly, and then allow them to cool as a unit to achieve cooling rates consistent with the spatter deposits at Devil's Garden, as determined by the strengths of their welds. Consequently, the estimated accumulation rates are likely a maximum as spatter-producing eruptions can sometimes be periodic in the location clast deposition. Consequently, the estimated accumulation rates are likely a maximum

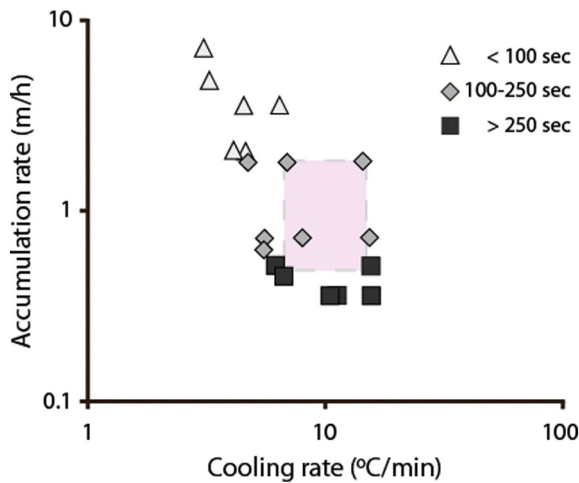


**Fig. 7.** Model results for cooling and accumulation rates for 5 cm clasts, which is representative of clasts in the Blowouts at Devil's Garden. The symbols represent the frequency of deposition of clasts, the higher the frequency, the higher the accumulation rate. Light grey triangles represent runs with less than 100 s between clasts, dark grey diamonds: 100–250 s, and black squares: intervals of greater than 250 s. The box outlines our estimates of the cooling regime of the natural samples from Devil's Garden.

value as the periodicity of spatter-producing eruptions results in bursts of deposition followed by less vigorous activity.

#### 4.3. Constraints on eruption of spatter

Accumulation rate and its influence on cooling rate of the deposit are thought to be the principal controls on the ability for pyroclasts to fuse. Differing amounts of fusion result in a variety of morphologies such as spatter, scoria, lava, or clastogenic lava (Fig. 8; Sumner et al., 2005; Head and Wilson, 1989). This study provides a constraint on spatter accumulation and cooling rates capable of producing a deposit of fluid, agglutinated clasts (Type 3, as defined by Sumner et al. (2005)). Deposits constituted of Type 3 scoria clasts likely require accumulation of 0.5–1.8 m/h of 5 cm clasts and cooling rates of 6.8 °C/min–14.3 °C/min, although local differences in these figures can be three times these values. If accumulation rates are greater than ~2 m/h, rheomorphism is likely to ensue, and clastogenic lava produced. At accumulation rates of <0.5 m/h, unwelded bomb and scoria deposits are likely to be produced, irrespective of the temperature of the clast upon impact. For the Blowouts, this translates into at least 13.3 h of spatter production and possibly as

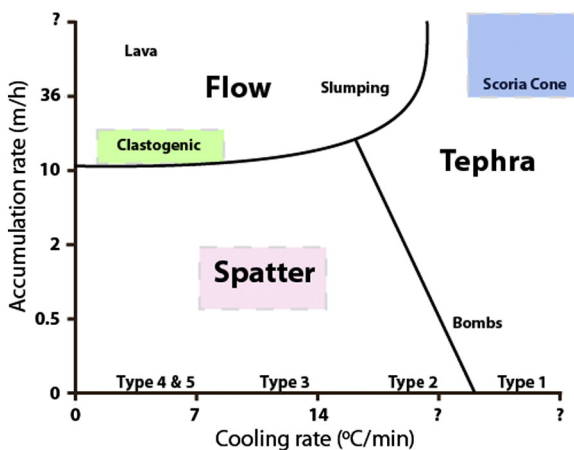


**Fig. 8.** Schematic diagram for explosive basaltic products modified from Sumner et al., 2005. The cooling and accumulation rates from the spatter (pink box) in this study, clastogenic estimates from Sumner (1998) in the green box, and scoria cone calculations (Riedel et al., 2003; Bemis et al., 2011) in the blue box allow us to assign values to this diagram. The exact locations of the lines are not yet known, and the axis are not yet to scale.

much as 40 h during the eruption at Devil's Garden. Heat loss to the atmosphere during transport can also affect these estimations but is not thought to strongly affect most proximal deposits because the spatter cones and ramparts are within 10–50 m of the vent (e.g. Capaccioni and Cuccoli, 2005).

#### 5. Conclusions

Basaltic spatter deposits consist of partly agglutinated clasts that can be individually recognized in the deposit. The clasts are deformed, indicating deposition in a plastic or semi-molten state, but they are not so hot that they remobilize as lava. We have been able to simulate the agglutination of spatter clasts experimentally by varying the cooling rate of hot basalt fragments. Comparisons of the weld strength between natural and experimental samples allows for a cooling rate to be calculated, ranging from 6.8 °C/min to 14 °C/min (with two outliers of 2.5 °C/min and 48 °C/min) for the Blowouts, a spatter rampart at Devil's Garden. A 1-D, finite difference model simulates the thermal evolution of a thickening spatter deposit. Eruptive conditions that result in the cooling rates we estimate for Devil's Garden yield maximum accumulation rates for 5-cm-thick clasts between 0.5 and 1.8 m/h. The time needed to build the 20-m-high spatter cones at the Blowouts would be somewhere between 13.3 and 40 h of explosive activity, whereas the 1.5-m hornito may have formed as quickly as 50 min or as long as 3 h. Stronger constraints on accumulation and cooling conditions will allow for new interpretations of eruption rates of the numerous basaltic eruptions that produce spatter. Additionally, eruptions that deposit spatter at accumulation rates as low as 2 m/h could be identified as a source of rheomorphic clastogenic lava and should be managed accordingly.

#### Acknowledgements

This work was funded by NSF grant EAR-0838153 to D. Geist and 0838171 to K. Harpp. Assistance with modeling was provided by E. Mittelstaedt. Thank you to the helpful comments by reviewers T. Orr and K. Putirka, which greatly improved the clarity of the manuscript as well as the editor M. Mangan.

#### References

- Bemis, K., Walker, J., Borgia, A., Turrin, B., Neri, M., Swisher, C., 2011. The growth and erosion of cinder cones in Guatemala and El Salvador: models and statistics. *J. Volcanol. Geotherm. Res.* 201 (1), 39–52.
- Bowles, J., Gee, J.S., Kent, D.V., Bergmanis, E., Sinton, J., 2005. Cooling rate effects on paleointensity estimates in submarine basaltic glass and implications for dating young flows. *Geochim. Geophys. Geosyst.* 6 (7).
- Capaccioni, B., Cuccoli, F., 2005. Spatter and welded air fall deposits generated by fire-fountaining eruptions: Cooling of pyroclasts during transport and deposition. *J. Volcanol. Geotherm. Res.* 145 (3–4), 263–280.
- Cashman, K.V., Thornber, C., Kauahikaua, J.P., 1999. Cooling and crystallization of lava in open channels, and the transition of Pahoehe Lava to A'a. *Bull. Volcanol.* 61 (5), 306–323.
- Chitwood, L.A., 1994. Inflated basaltic lava—examples of processes and landforms from central and southeast Oregon. *Or. Geol.* 56, 11–21.
- Christiansen, R.L., Foulger, G.R., Evans, J.R., 2002. Upper-mantle origin of the Yellowstone hotspot. *Geol. Soc. Am. Bull.* 114 (10), 1245–1256.
- Davies, A.G., Keszhelyi, L., McEwen, A.S., 2011. Estimating eruption temperature from thermal emission spectra of lava fountain activity in the Erta'Ale (Ethiopia) volcano lava lake: Implications for observing Io's volcanoes. *Geophys. Res. Lett.* 38 (21).
- Einarsson, T., 1966. Studies of temperature, viscosity, density and some types of materials produced in the Surtsey eruption. *Surtsey Res. Prog. Rep.* 2, 163–179.
- Erickson, M.S., Hopkins, R.T., Fey, D.L., King, H.D., 1989. Analytical results and sample locality map of rock samples from the Devil's Garden Lava Bed (OR-1-2), Squaw Ridge Lava Bed (OR-1-3), and Four Craters Lava Bed (OR-1-22) Wilderness Study Areas, Lake County, Oregon. USGS Open-File Report. 89-307 pp. 1–10.
- Fagents, S.A., 1996. Emplacement Mechanisms of Volcanic Materials on Mars. *Lunar and Planetary Institute Science Conference Abstracts* 27, p. 349.
- Fagents, S.A., Wilson, L., 1994. Theoretical analysis of the explosive emplacement of basaltic magma in lava fountain eruptions: implications for pyroclast dispersal on Earth, Venus and Mars. *Lunar and Planetary Institute Science Conference Abstracts* 25, p. 361.
- Gerya, T., 2010. *Introduction to Numerical Geodynamic Modelling*. Cambridge University Press.

- Giordano, D., Nichols, A., Dingwell, D., 2005. Glass transition temperatures of natural hydrous melts: a relationship with shear viscosity and implications for the welding process. *J. Volcanol. Geotherm. Res.* 142 (1–2), 105–118.
- Gottsmann, J., Dingwell, D., 2001. Cooling dynamics of spatter-fed phonolite obsidian flows on Tenerife, Canary Islands. *J. Volcanol. Geotherm. Res.* 105 (4), 323–342.
- Gottsmann, J., Harris, A.J., Dingwell, D.B., 2004. Thermal history of Hawaiian pahoehoe lava crusts at the glass transition: implications for flow rheology and emplacement. *Earth Planet. Sci. Lett.* 228 (3), 343–353.
- Harris, A.J., Carniel, R., Jones, J., 2005. Identification of variable convective regimes at Erta Ale lava lake. *J. Volcanol. Geotherm. Res.* 142 (3), 207–223.
- Hauber, E., Bleacher, J., Gwinner, K., Williams, D., Greeley, R., 2009. The topography and morphology of low shields and associated landforms of plains volcanism in the Tharsis region of Mars. *J. Volcanol. Geotherm. Res.* 185 (1), 69–95.
- Head, J.W., Wilson, L., 1989. Basaltic pyroclastic eruptions: influence of gas-release patterns and volume fluxes on fountain structure, and the formation of cinder cones, spatter cones, rootless flows, lava ponds and lava flows. *J. Volcanol. Geotherm. Res.* 37 (3–4), 261–271.
- Jordan, B.T., Grunler, A.L., Duncan, R.A., Deino, A.L., 2004. Geochronology of age-progressive volcanism of the Oregon High Lava Plains: implications for the plume interpretation of Yellowstone. *J. Geophys. Res. Solid Earth* (1978–2012) 109 (B10).
- Keith, W.J., King, H.D., Gettings, M.E., Johnson, F.L., 1988. Mineral resources of the Devil's Garden lava bed, Squaw Ridge lava bed, and Four Craters lava bed wilderness study areas, Lake County, Oregon. *U.S. Geol. Surv. Bull.* A1–A14.
- Nichols, A., Potuzak, M., Dingwell, D., 2009. Cooling rates of basaltic hyaloclastites and pillow lava glasses from the HSDP2 drill core. *Geochim. Cosmochim. Acta* 73 (4), 1052–1066.
- Riedel, C., Ernst, G., Riley, M., 2003. Controls on the growth and geometry of pyroclastic constructs. *J. Volcanol. Geotherm. Res.* 127 (1), 121–152.
- Robertson, E.C., 1988. *Thermal Properties of Rocks*. US Department of the Interior, Geological Survey.
- Robertson, E.C., Peck, D.L., 1974. Thermal conductivity of vesicular basalt from Hawaii. *J. Geophys. Res.* 79 (32), 4875–4888.
- Sigurðsson, T., 1966. Geophysical measurements in Surtsey carried out during the year of 1965. *Surtsey Res. Prog. Rep.* 2, 181–185.
- Sumner, J.M., 1998. Formation of clastogenic lava flows during fissure eruption and scoria cone collapse: the 1986 eruption of Izu-Oshima Volcano, eastern Japan. *Bull. Volcanol.* 60, 195–212.
- Sumner, J., Blake, S., Matela, R., Wolff, J., 2005. Spatter. *J. Volcanol. Geotherm. Res.* 142 (1–2), 49–65.
- Thomas, R.M.E., Sparks, R.S.J., 1992. Cooling of tephra during fallout from eruption columns. *Bull. Volcanol.* 54 (7), 542–553.
- Wilding, M., Webb, S., Dingwell, D., Ablay, G., Marti, J., 1996. Cooling rate variation in natural volcanic glasses from Tenerife, Canary Islands. *Contrib. Mineral. Petrol.* 125 (2–3), 151–160.
- Wolfe, E.W., 1988. The Puu Oo eruption of Kilauea Volcano, Hawaii; episodes 1 through 20, January 3, 1983, through June 8, 1984. 1463.
- Zdanowicz, C.M., Zielinski, G.A., Germani, M.S., 1999. Mount Mazama eruption: calendrical age verified and atmospheric impact assessed. *Geology* 27 (7), 621–624.